Biaxial strain-modified valence and conduction band offsets of zinc-blende GaN, GaP, GaAs, InN, InP, and InAs, and optical bowing of strained epitaxial InGaN alloys

P. R. C. Kent, Gus L. W. Hart, and Alex Zunger[a)]
National Renewable Energy Laboratory, Golden, Colorado 80401

(Received 3 July 2002; accepted 2 October 2002)

Using density-functional calculations, we obtain the (001) biaxial strain dependence of the valence and conduction band energies of GaN, GaP, GaAs, InN, InP, and InAs. The results are fit to a convenient-to-use polynomial and the fits provided in tabular form. Using the calculated biaxial deformation potentials in large supercell empirical pseudopotential calculations, we demonstrate that epitaxial strain reduces the InGaN alloy bowing coefficient compared to relaxed bulk alloys. © *2002 American Institute of Physics.* [DOI: 10.1063/1.1524299]

The energy of the conduction band minimum (CBM) and valence band maximum (VBM) of common zinc-blende semiconductors can be altered[1] via hydrostatic pressure,[2] epitaxy-induced biaxial strain,[3–6] or alloying.[7] These energy changes are important parameters needed for the quantum design of electronic nanostructures. The rate of change of CBM and VBM energies with hydrostatic pressure (''absolute pressure deformation potentials'') is summarized in Ref. 2 for many common binary semiconductors. However, reliable absolute *biaxial* deformation potentials are less common (e.g., Refs. 4 and 6). Here, we provide easy to use, fitted numerical results of the variation with (001) strain of the VBM and CBM energies of zinc-blende GaN, GaP, GaAs, InN, InP, and InAs, obtained from first-principles local-density calculations.

The VBM of zinc-blende materials consists of degenerate bands (two-fold Γ_{8v} and one-fold Γ_{7v}) and, therefore, their response to strain is complex.[8] Previously, first-order, linear in strain, perturbation models within the envelope function approximation have been used.[3,7] Here, we calculate the band structure of each strained system self-consistently, so our results are not limited to small strains, envelope function approximations, or to low-order perturbative treatments of the strain-mediated interband coupling. Once obtained, the VBM and CBM energies are fit to a low-order polynomial in strain. Together with the InX/GaX (X=N,P,As) *unstrained* valence band offset (tabulated in Ref. 9 for all common semiconductors), our results give the band offsets between InX/GaX at any intermediate (001) strain (i.e., corresponding to a substrate with in-plane lattice constant between that of InX and GaX).

The band structure and tetragonal deformations of strained zinc-blende materials were calculated in the local-density approximation using the linear augmented plane wave (LAPW) approach[10,11] (*WIEN*97 implementation),[12] including spin–orbit effects. We use the exchange correlation of Perdew and Wang.[13] For each in-plane (001) lattice constant $a_{\mathrm{In}X} \leqslant a_{\text{in-plane}} \leqslant a_{\mathrm{Ga}X}$, we minimize the total energy with respect to the tetragonal distortion c/a. The band structure is then computed at $[a_{\text{in-plane}};\ (c/a)_{\mathrm{eq}}]$ for a range of $a_{\text{in-plane}}$ values. To separate the movement of the VBM and CBM, we use the energy of the lowest 1s states as a reference. (This is similar to both the experimental photoemission spectroscopy approach[14,15] and first-principles calculational approach[16] to determining band offsets.) Although we use the local-density approximation for the conduction states, which are subject to the band gap error, we expect the *change* in the conduction state energies with lattice constant to be accurate.

The results for InP/GaP are plotted in Fig. 1 where we have aligned the unstrained eigenvalues using the *calculated* valence band offset[9] and the unstrained *experimental* band gaps.[17] Results are fit to polynomials of the form

$$E_{\mathrm{SO}} = \Delta_{\mathrm{so}} + C_1 x + C_2 x^2 + C_3 x^3, \tag{1}$$

$$E_{\mathrm{HH}} = C_1 x + C_2 x^2 + C_3 x^3, \tag{2}$$

$$E_{\mathrm{LH}} = C_1 x + C_2 x^2 + C_3 x^3, \tag{3}$$

$$E_{\mathrm{CBM}} = E_{\mathrm{gap}} + C_1 x + C_2 x^2 + C_3 x^3, \tag{4}$$

where $x \equiv (a_{\mathrm{epi}} - a_0)$, a_{epi} is the in-plane lattice constant, a_0 is the cubic equilibrium lattice constant (in Å), Δ_{so} is the spin–orbit splitting at the VBM interaction, and E_{gap} is the band gap (in eV). This form for the band-edge states gives

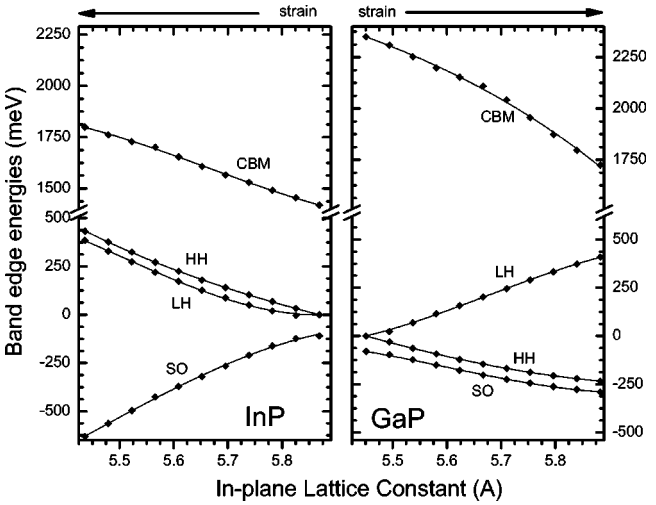

FIG. 1. LAPW calculated CBM and VBM states (indicated by points) for cubic GaP and InP for substrate lattice constants $a_{\mathrm{GaP}} \leqslant a_{\text{in-plane}} \leqslant a_{\mathrm{InP}}$. The corresponding fits from Table I are shown by solid lines.

a)Electronic mail: azunger@nrel.gov

TABLE I. LDA fitted results according to Eqs. (1)–(4). The HH and LH states are labeled assuming the same valence band structure as InAs and GaAs.

Band-edge state		Parameters		
		C_1	C_2	C_3
GaN	SO	−558.0	1132.7	−452.8
	LH	1668.0	−416.7	327.3
	HH	−593.9	1385.1	−744.4
	CBM	−1071.6	1553.2	−1122.8
InN	SO	1584.7	228.5	1158.4
	LH	−602.3	286.3	−1073.9
	HH	−674.7	157.6	−1190.0
	CBM	−79.9	1748.3	1426.6
GaP	SO	−469.5	−765.9	1699.0
	LH	678.5	1686.7	−2488.2
	HH	−777.8	433.3	274.7
	CBM	−972.2	−788.9	−814.1
InP	SO	475.0	−2748.5	−2437.0
	LH	6.8	3448.3	3155.4
	HH	−769.5	219.5	−797.5
	CBM	−760.0	1020.0	1731.1
GaAs	SO	−245.1	−959.9	1349.4
	LH	531.1	531.6	−439.6
	HH	−822.6	533.5	−151.6
	CBM	−1828.7	469.6	−244.9
InAs	SO	−53.9	−3651.6	−2364.5
	LH	594.3	3412.6	2842.0
	HH	−873.7	−778.3	−1498.4
	CBM	−166.3	2515.7	4086.9

the VBM as zero energy. The values for a_0, Δ_{so}, and E_{gap} can all be taken from the experiment; our fits provide the coefficients C_i. These coefficients are given in Table I, and the values of a_0, Δ_{so}, and E_{gap} are given in Table II.

In Fig. 2 we have plotted the difference (band offset) in light hole (LH), heavy hole (HH), and split-off (SO) energies betweeen GaP and InP versus lattice constant. From this, we can see that while the unstrained LH and HH offsets between GaP and InP are 110 meV, these change to 41 meV and 438 meV (for the LH and HH, respectively) when GaP and InP are grown on a GaAs substrate (indicated by the vertical dotted line in Fig. 2). Similarly, the offset for the SO states changes from −20 to −190 meV. We show the LAPW calculated CBM, VBM, and fitted results for InAs/GaAs in Fig. 3, and for InN/GaN in Fig. 4.

The strain-modified band-edge energies are important for understanding the difference in alloy optical bowing of

TABLE II. Experimental lattice constants and band structure parameters (from Ref. 17).

Material	Parameters		
	a_0 (A)	Δ_{SO} (meV)	E_{gap} (eV)
GaN	4.508	11	3.5
InN	4.979	11	1.9
GaP	5.451	80	2.35
InP	5.869	110	1.42
GaAs	5.652	340	1.519
InAs	6.058	380	0.418

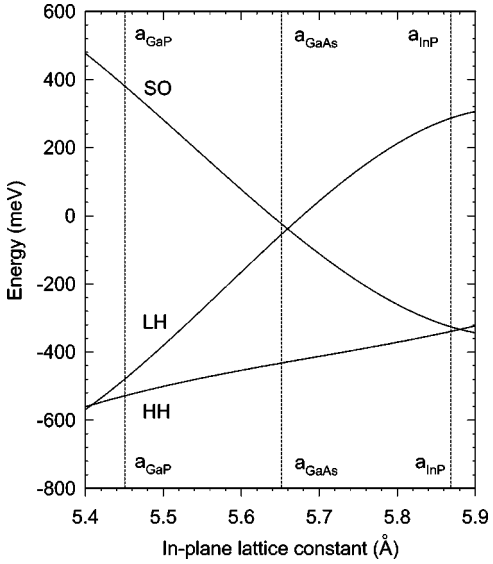

FIG. 2. Valence band offsets between GaP and InP for substrate lattice constants $a_{GaP} \leqslant a_{in\text{-}plane} \leqslant a_{InP}$, for LH, HH, and SO states.

freestanding, relaxed ''bulk'' systems and epitaxially strained films. To illustrate this, we examined the case of cubic $In_xGa_{1-x}N$ under bulk and epitaxial (on GaN) conditions. We first calculated the composition variation of the VBM and CBM energies of the bulk alloys. We generated strain-dependent empirical pseudopotentials following the procedure of Ref. 18. Specifically, the potentials were fitted to the local density approximation calculated absolute pressure and biaxial deformation potential (described herein), as well as to the measured band structure. The bulk alloy was modeled by a translationally repeated 13824 atom cubic supercell whose 6912 cation sites are randomly occupied by In and Ga atoms, while all the nitrogen atoms are placed at their proper tetrahedral site. Atomic positions were relaxed by minimizing the strain energy while keeping the overall lattice constant at its Vegard value. The band structure was calculated using a plane-wave basis, and the resulting band-edge energies averaged over five randomly selected supercell configurations. The solid lines in Fig. 5(a) show the band-edge energies, and

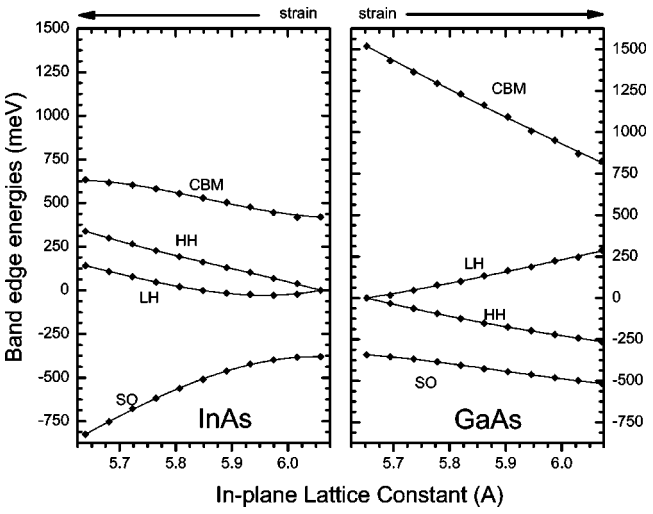

FIG. 3. LAPW calculated CBM and VBM states (indicated by points) for cubic GaAs and InAs for substrate lattice constants $a_{GaAs} \leqslant a_{in\text{-}plane} \leqslant a_{InAs}$. The corresponding fits from Table I are shown by solid lines.

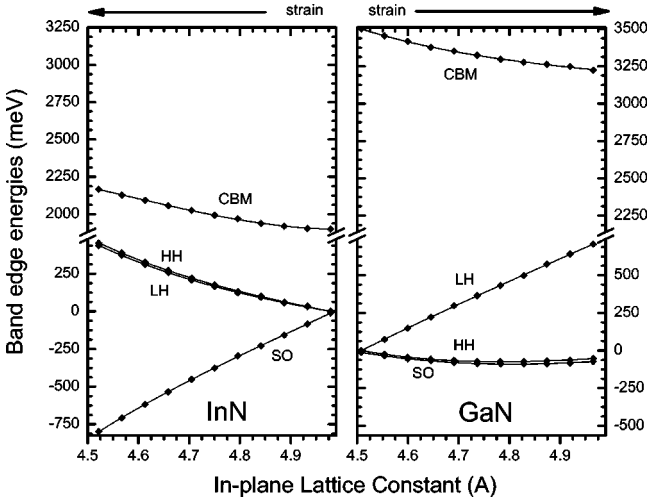

FIG. 4. LAPW calculated CBM and VBM states (indicated by points) for cubic GaN and InN for substrate lattice constants $a_{\mathrm{GaN}} \leqslant a_{\text{in-plane}} \leqslant a_{\mathrm{InN}}$. The corresponding fits from Table I are shown by solid lines. The unstrained valence band offset between InN and GaN is 260 meV.

are quantitatively similar to Bellaiche *et al.*[19] except for improved statistics in the present work. The strong upward shift of the VBM for indium concentrations $<10\%$ is consistent with recent x-ray measurements.[20] In Fig. 5(b), we show the band gap bowing coefficient assuming a gap of 1.9 eV for InN. We see that the bowing coefficient is composition dependent and is large and positive, $\geqslant 4$ eV, for indium compositions below 10%, due to the strong upward bowing of the VBM. For higher indium compositions, the bowing is reduced to 2–3 eV. When we assume in our pseudopotential fit that InN has a gap of 0.8 eV, the bowing coefficient is reduced significantly for both bulk and epitaxial film but the *relative* bowing is unchanged.

To model the epitaxial alloy grown on GaN, we confined the in-plane lattice constant of the $\mathrm{In}_x\mathrm{Ga}_{1-x}\mathrm{N}$ alloy to that of GaN, relaxing the c/a ratio and all atomic positions. The band-edge energies, obtained using the same method as for the bulk alloys, are shown in Fig. 5(a) as dashed lines. Now the bowing coefficients are reduced, compared to the bulk, for indium compositions up to $\sim 30\%$, e.g., $b=2.8$ versus 3.4 eV for the epitaxial and bulk bowing coefficient at $x=0.20$. In Ref. 21, a reduction in bowing coefficient due to expitaxy of 0.7 eV was measured for $x<0.25$.

To understand the effect of epitaxy-reduced alloy bowing, we refer again to Fig. 4. We see that compressing InN biaxially to the in-plane lattice constant of GaN raises the VBM energy by 480 meV and also raises the CBM by 350 meV, so the epitaxial gap is only 130 meV lower than the bulk InN gap. At the other end of the composition range, $x=0$, the bulk and epitaxial gaps are identical. As the In composition increases from $x=0$, the epitaxial alloy reduces its band gap by a lesser amount than the bulk alloy since the GaN component has a *higher* VBM, while the InN component has a *lower* VBM with increasing $a_{\text{in-plane}}$. On the other hand, the CBM of both the GaN and InN components decrease as $a_{\text{in-plane}}$ increases. However, the CBM of the bulk alloy decreases faster than that of the epitaxial alloys. *Consequently, the epitaxial alloy has a smaller optical bowing than the bulk alloy*. This observation shows that larger bowing is expected in relaxed, bulklike samples, while epitaxial samples should have ~ 0.5 eV lower bowing parameters, for the device-relevant indium composition range of $\leqslant 30\%$. This holds for InN gap of either 1.9 or 0.8 eV.

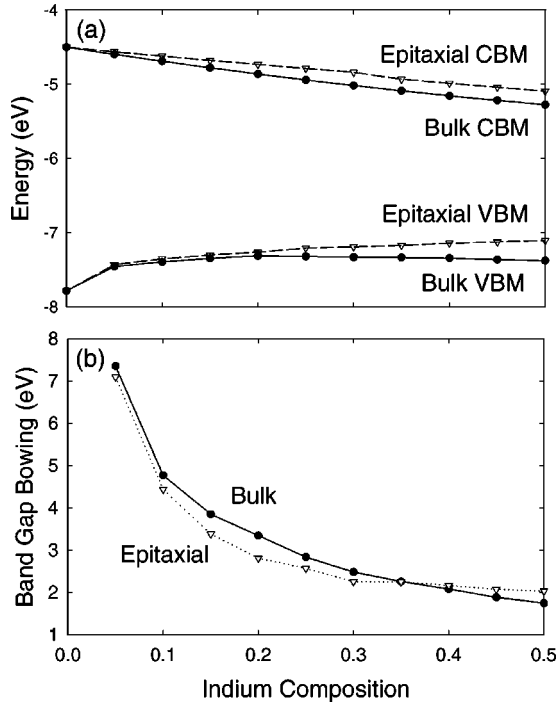

FIG. 5. Band edges and band gap bowing of bulk and epitaxially strained InGaN calculated using the empirical pseudopotential method, assuming a gap of l.9 eV for InN.

This work is supported by the U.S. Department of Energy, SC-BES-OER Grant No. DE-AC36-98-GO10337.

[1] P. Y. Yu and M. Cardona, *Fundamentals of Semiconductors* (Springer, New York, 1996).
[2] S.-H. Wei and A. Zunger, Phys. Rev. B **60**, 5404 (1999).
[3] F. H. Pollak and M. Cardona, Phys. Rev. **172**, 816 (1968).
[4] C. G. Van de Walle and M. Martin, Phys. Rev. B **34**, 5621 (1986).
[5] S.-H. Wei and A. Zunger, Phys. Rev. B **57**, 8983 (1998).
[6] C. G. Van de Walle, Phys. Rev. B **39**, 1871 (1989).
[7] G. L. Bir and G. E. Pikus, *Symmetry and Strain-Induced Effects in Semiconductors* (Wiley, New York, 1974).
[8] Y. Zhang, Phys. Rev. B **49**, 14352 (1994).
[9] S.-H. Wei and A. Zunger, Appl. Phys. Lett. **72**, 2011 (1998).
[10] S.-H. Wei and H. Krakauer, Phys. Rev. Lett. **55**, 1200 (1985), and references therein; D. J. Singh, *Planewaves, Pseudopotential, and the LAPW Method* (Kluwer, Boston, 1994), and references therein.
[11] D. J. Singh, Phys. Rev. B **43**, 6388 (1991).
[12] P. Blaha, K. Schwarz, and J. Luitz, *WIEN*97, Vienna University of Technology, Vienna, 1997; Updated version of P. Blaha, K. Schwarz, P. Sorantin, and S. B. Trickey, Comput. Phys. Commun. **59**, 399 (1990).
[13] J. P. Perdew and Y. Wang, Phys. Rev. B **45**, 13 244 (1992).
[14] S. P. Kowalczyk, J. T. Cheung, E. A. Kraut, and R. W. Grant, Phys. Rev. Lett. **56**, 1605 (1986); C. Hsu and J. P. Faurie, *ibid.* **58**, 1127 (1987).
[15] T. M. Duc, C. Hsu, and J. P. Faurie, Phys. Rev. Lett. **58**, 1127 (1987).
[16] G. L. W. Hart and A. Zunger, Phys. Rev. B **62**, 13522 (2000).
[17] Landolt-Börnstein, *Numerical Data and Functional Relationships in Science and Technology*, (Springer, Berlin, 1987), Vol. 22a.
[18] K. Kim, P. R. C. Kent, A. Zunger, and C. B. Geller, Phys. Rev. B **66**, 045208 (2002).
[19] L. Bellaiche, T. Mattila, L.-W. Wang, S.-H. Wei, and A. Zunger, Appl. Phys. Lett. **74**, 1842 (1999).
[20] P. Ryan, C. McGuinness, J. E. Downes, and K. E. Smith, Phys. Rev. B **65**, 205201 (2002).
[21] C. A. Parker, J. C. Roberts, S. M. Bedair, M. J. Reed, S. X. Liu, N. A. El-Masry, and L. H. Robins, Appl. Phys. Lett. **75**, 2566 (1999).